Limits to Mercury's magnesium exosphere from MESSENGER second flyby observations

Menelaos Sarantos[a,b,*], Rosemary M. Killen[c], William E. McClintock[d], E. Todd Bradley[e], Ronald J. Vervack, Jr.[f], Mehdi Benna[b,g], and James A. Slavin[a]

[a] Heliophysics Science Division, NASA Goddard Space Flight Center, Greenbelt, MD 20771, USA

[b] Goddard Earth Sciences and Technology Center, University of Maryland, Baltimore County, Baltimore, MD 21228, USA

[c] Planetary Magnetospheres Branch, NASA Goddard Space Flight Center, Greenbelt, MD 20771, USA

[d] Laboratory for Atmospheric and Space Physics, University of Colorado, Boulder, CO 80303, USA

[e] Department of Physics, University of Central Florida, Orlando, FL 32816, USA

[f] The Johns Hopkins University Applied Physics Laboratory, Laurel, MD 20723, USA

[g] Solar System Exploration Division, NASA Goddard Space Flight Center, Greenbelt, MD 20771, USA

*Corresponding author. Fax: +1 301 286 1648. Phone: +1 301 286 2945

E-mail address: menelaos.sarantos-1@nasa.gov

Abstract

The discovery measurements of Mercury's exospheric magnesium, obtained by the MErcury Surface, Space ENvironment, GEochemistry, and Ranging (MESSENGER) probe during its second Mercury flyby, are modeled to constrain the source and loss processes for this neutral species. Fits to a Chamberlain exosphere reveal that at least two source temperatures are required to reconcile the distribution of magnesium measured far from and near the planet: a hot ejection process at the equivalent temperature of several tens of thousands of degrees K, and a competing, cooler source at temperatures as low as 400 K. For the energetic component, our models indicate that the column abundance that can be attributed to sputtering under constant southward interplanetary magnetic field (IMF) conditions is at least a factor of five less than the rate dictated by the measurements. Although highly uncertain, this result suggests that another energetic process, such as the rapid dissociation of exospheric MgO, may be the main source of the distant neutral component. If meteoroid and micrometeoroid impacts eject mainly molecules, the total amount of magnesium at altitudes exceeding ~100 km is found to be consistent with predictions by impact vaporization models for molecule lifetimes of no more than two minutes. Though a sharp increase in emission observed near the dawn terminator region can be reproduced if a single meteoroid enhanced the impact vapor at equatorial dawn, it is much more likely that observations in this region, which probe heights increasingly near the surface, indicate a reservoir of volatile Mg being acted upon by lower-energy source processes.

Keywords:

Mercury

Mercury atmosphere

Mercury surface

Atmospheric structure

Mercury magnetosphere

MESSENGER

1. Introduction

Mercury is enveloped by a rarefied collisionless exosphere whose source is largely the surface of the planet itself, which is continuously being bombarded by a flux of micrometeoroids, solar-wind ions, and ultraviolet (UV) photons. Known exospheric constituents include H, He, Na, K, O, and Ca (e.g., Killen et al., 2007), and Mg, which was recently discovered by the MErcury Surface, Space ENvironment, GEochemistry, and Ranging (MESSENGER) spacecraft (McClintock et al., 2009). Because the exosphere reflects a combination of surface composition, the composition of vaporizing micrometeoroids, and the escape rates of atoms from the various source processes, we expect the detection of other atomic and molecular constituents of Mercury's exosphere by MESSENGER (Solomon et al., 2001) and by future missions such as BepiColombo (Milillo et al., 2010).

On its way to insertion into orbit around Mercury in 2011, MESSENGER flew by the planet three times, on January 14, 2008, October 6, 2008, and September 29, 2009. During the first of these encounters (M1), the Ultraviolet and Visible Spectrometer (UVVS) channel on the Mercury Atmospheric and Surface Composition Spectrometer (MASCS) instrument on MESSENGER observed the planet's exosphere at the resonant emission lines of Na (589.0 and 589.5 nm), Ca (422.7 nm), and H (121.6 nm) (McClintock et al., 2008). During the second (M2) and third (M3) flybys, UVVS also observed the Mg (285.2 nm) line (McClintock et al., 2009; Vervack et al., 2010). MESSENGER probed the nightside (tail) and terminator exospheric regions with unprecedented spatial coverage but did not observe the dayside exosphere (except for H). These observations revealed substantial differences even for chemically related species. Calcium appeared to peak near the equatorial dawn flank during all three flybys, sodium was enhanced at high latitudes, and magnesium appeared to be uniformly distributed during M2 but enhanced above the northern pole during M3.

The differences in the distributions of individual species point to differing ejection mechanisms and relate, perhaps, to different regions of surface composition and/or mechanisms of global circulation and surface replenishment. Sodium has been the most extensively studied species because its favorable spectroscopic properties enable its long-term monitoring from Earth, yet the relative importance of several proposed source processes is still under debate (e.g, Killen et al., 2001; Killen et al., 2004, Mura et al., 2009) and their interplay may exhibit an annual trend (Leblanc and Johnson, 2010). At the time of the MESSENGER flybys, the main source of low-latitude sodium production was found to be photon-stimulated desorption (PSD); the efficiency of this source was enhanced at high latitudes by solar wind precipitation (Burger et al., 2010); finally, the dayside content was consistent with a moderate degree of thermal accommodation upon interaction with the surface (Mouawad et al., 2011). Although the calcium distribution obtained by MESSENGER remains unexplained, its high temperature in the tail is consistent with the possible photodissociation of an exospheric molecule such as CaO as suggested by ground-based observations (Killen et al., 2005).

The measurements of Mg by MESSENGER were first analyzed by Killen et al. (2010). They showed that the observed magnesium tail was hotter than can be expected by direct impact vaporization, and they attributed these high temperatures (>10,000 K) to vaporization of ~30% of the magnesium vapor in molecular form (MgO) followed by its dissociation. They noted that the exospheric temperature was poorly constrained, even more so near the planet, where no single temperature could be made to fit. In this paper we elaborate upon the Killen et al. (2010) analysis using a large number of simulations that seek to constrain many unknown physical constants for this species, such as the lifetime of the proposed molecule, the inferred exospheric source rates, and the relation between the exosphere and the surface content. In Sections 2 and 3 we describe the observational sequence, we analyze the measurements using a Chamberlain (1963) model, and we provide evidence of multiple source components and rates. In Section 4 we detail our exosphere model assumptions and place limits on the possible contributions from several proposed source processes of exospheric magnesium: (1) solar-wind ion sputtering in polar areas that are only partially shielded by the planetary magnetic field, (2) production of magnesium atoms due to micrometeoroid impact vaporization, and (3) dissociation of a Mg-bearing molecule such as MgO with a finite lifetime. In Section 5 we demonstrate that low-altitude data obtained near the dawn terminator strongly suggest the presence of either an additional local source or, more likely, a source that is colder than impacts or sputtering. The paper concludes with a summary of the major findings in Section 6.

2. Observations of magnesium during the second MESSENGER flyby

Sean Solomon 3/4/11 9:16 AM
Comment:

During the second MESSENGER flyby, the UVVS spectrometer scanned Mercury's exosphere at the Mg 285.2-nm line with a 0.1° × 1° field of view. The measurements, detailed by McClintock et al. [2009], were organized spatially and temporally in the following sequence:

- As the spacecraft approached Mercury and at downstream distances between 14 R_M and 2 R_M (where R_M is Mercury's radius, or 2,440 km), both the equatorial and the high-latitude neutral tail were observed.
- While inside Mercury's shadow (and near closest approach), the spacecraft executed a ~180° roll, initially pointing toward dawn, then rotating through north toward the dusk direction, while moving toward the planet from about 3,000 km (1.2 R_M) to within 450 km (0.2 R_M) above the planetary surface.
- As the spacecraft exited the shadow past closest approach and at distances ≤ 1,000 km, the lines of sight pointed toward the planetary shadow and intersected the surface in the equatorial near-nightside and dawn terminator regions.

In what follows we refer to the set of observations obtained first upon initial approach to Mercury as "tail measurements," to the set of observations obtained second during the spacecraft roll as "fantail measurements," and to the third and final set as "near-terminator measurements." Observations of magnesium on the dayside were not conducted during the flybys. The excitation mechanism is presumed to be resonant scattering of sunlight. Hence, the instrument sees that portion of the exosphere that is illuminated, i.e., outside Mercury's shadow.

Excepting the shadow, the tail and fantail lines of sight probed exospheric material from the spacecraft to infinity. During these two sequences the closest tangent point outside the shadow was ~1100 km above the surface. Because the minimum ejection speed for a magnesium atom to reach this altitude is 2.3 km/s, or ~50% of the escape velocity, these lines of sight survey energetic atoms. In marked contrast, the measurements near the dawn terminator probed material much closer to the surface, with lines intercepting the shadow at progressively diminishing heights, starting at 162 km altitude and eventually reaching the surface. Obviously, a wider spectrum of ejection speeds can populate these altitudes compared to altitudes scanned by the tail and fantail observations. Another difference is that lines of sight near the terminator are only 200–800 km long (i.e., from the spacecraft to the shadow or surface).

3. Fits to a Chamberlain exosphere

In order to remove geometrical effects, the exospheric measurements were first fit to a Chamberlain (1963) model. The instrument measures intensity,

$$4\pi I = gN_{LOS} = \int_{R_{SP}}^{\infty} g(\mathbf{r})n(\mathbf{r})\, ds, \qquad (1)$$

where g is the emission probability (photons s^{-1} atom^{-1}) at the relevant Doppler-shifted resonance line, N_{LOS} is the column abundance, $\mathbf{r}$ is the radius vector from the planet center, s is the distance along the line of sight (LOS) from the spacecraft location R_{SP} to infinity (or to the shadow in the case of the measurements near the terminator), and the neutral density n is a function of altitude and source temperature. Two model free parameters must be determined by least squares fitting of the model to the data weighted by the measurement uncertainty: the temperature, T, and the surface density, n_0, of the source. We have run models having with exobase temperatures between 100 K and 50,000 K and have excluded from the model intensities, I, the portion lying inside the planetary shadow.

Comparisons of modeled and observed magnesium in the tail regions are presented in Fig. 1, followed, in Fig. 2, by fits of the fantail and near-terminator measurements. The modeled column abundances were converted to line intensity using a g–factor for Mg at 285.2 nm of g_{Mg} = 0.317 photons s^{-1} $atom^{-1}$ given Mercury's radial velocity of v_r = - 9.2 km/s during the flyby (Killen et al., 2009, 2010). The tail data (Fig. 1) are ordered by the distance $-x$ downstream of Mercury where each line of sight intercepts the noon–midnight meridian (x-z) plane, and by the distance z of this intercept above the equatorial plane. The fantail data (Fig. 2a) are shown versus the boresight angle with respect to dawn (where dawn = 0° and north = 90°), and the near-terminator lines (Fug. 2b) are plotted against the spacecraft altitude from the planetary shadow. The best-fit parameters, n_0 and T, for each model, along with the reduced chi-squared error, χ^2/ν (where ν is the number of measurements minus two) and the corresponding production rate of magnesium atoms, $S = \frac{n_0}{2\sqrt{\pi m/2K_B T}}$, for an assumed Maxwellian velocity distribution (where m is the mass of a magnesium atom and K_B is the Boltzmann constant), were computed using all ~200 lines of sight.

[Insert Fig.1; Fig.2]

Inspection of Figs. 1 and 2 leads to the following conclusions:

1) A single "warm" ($T \leq$ 10,000 K) source underestimates the tail measurements and overestimates data near the planet.
2) A single hot source can describe measurements obtained far from the planet with production rate ~(8–15) × 10^5 atoms cm^{-2} s^{-1}. Models having temperatures ≥ 20,000 K are indistinguishable given the uncertainty in the measurements (see Figs. 1 and 2).

3) No single temperature can describe the data near and far from the planet in an internally consistent manner. The rates and temperatures needed to fit the tail measurements underestimate the magnesium abundance near the surface.

These remarks effectively summarize the conclusions of the analysis by Killen et al. (2010). The improvement up to this point is that we have fit all measurements together here, a treatment that accentuates the conclusion of several distinct components.

In Fig. 3 we have fit the measurements in the weighted least-squares sense to a two-component Chamberlain model, $I(\mathbf{r}) = n_{0,LT}\, I(\mathbf{r}, T_{COOL}) + n_{0,HT}\, I(\mathbf{r}, T_{HOT})$, where $n_{0,LT}$ ($n_{0,HT}$) and T_{COOL} (T_{HOT}) are the surface density and temperature, correspondingly, of the cool (hot) components of the exosphere. In this case the added constraint of non-negative surface densities must be enforced in minimizing the squared residuals in order to obtain physically meaningful solutions. We have found that the superposition of a hot source ($T_{HOT} \geq 20{,}000$ K) with a cooler source ($T_{COOL} \leq 5000$ K) improves the description near dawn compared to residuals obtained with a single-component model (e.g., compare Figs. 2 and 3a-b and the related χ^2/ν error shown in Table 1 when $T_{COOL} = 3000$ K is assumed). In particular, Figs. 3c-d demonstrate that the exospheric signature at low altitudes is reproduced best if $T_{COOL} = 400$ K is assumed, which describes thermalized ejecta (also see Table 1). At $T = 400$ K the mean velocity of a magnesium atom leaving the surface is 1 km/s, so the altitude reached is ~152 km. Such a low-energy source is undetectable given only tail and fantail measurements, and lies below the scale of Fig. 3c.

[Insert Figure 3; Insert Table 1]

In conclusion, Chamberlain models indicate that at least two distinct temperatures and source rates of a few times 10^6 atoms cm^{-2} s^{-1} are required to fit the data. In the next section we investigate the kinds of physical processes that might be consistent with these requirements.

4. Relative roles of sources populating the magnesium tail

4.1. Model formulation

Mercury's neutrals are subject to losses via ballistic escape, radiation acceleration (strong for Na, weak for Ca, and negligible for Mg), adsorption upon surface impact, and photoionization. Thus, they are continuously resupplied by the surface via a number of processes, including photon-stimulated desorption and thermal desorption that act upon volatiles, as well as micrometeoroid impact vaporization and sputtering by the solar wind and recycled magnetospheric ions that act upon both volatile and refractory species (e.g., Killen et al., 2007).

Near Mercury the magnesium neutrals are subjected only to gravitational forces, because for this species the radiation pressure is a very small fraction of Mercury's gravity and the photoionization lifetime is ~ 57 h (McClintock et al., 2009). Hence, the magnesium production and its distribution are modeled with an analytical model of particle transport in a collision-free exosphere (Hartle, 1971). The model uses Liouville's theorem to compute the density of neutrals,

$$n(\mathbf{r}) = \int f(\mathbf{r}, \mathbf{v}) d^3\mathbf{v}, \qquad (2)$$

at an exospheric location $\mathbf{r}$, where f is a truncated distribution function relating the constants of motion in a gravitational field to $f_0(\mathbf{r_0}, \mathbf{v_0})$, the velocity distribution function of released particles from the surface. Prior to applying it to the study of magnesium transport at Mercury, we modified this model to simulate the velocity distribution function of sputtered particles, we used it to describe the source rates of the lunar sodium exosphere, and we validated it against ground-based observations (Sarantos et al., 2010).

4.1.1. Exospheric sources

The sources we initially considered are the typical processes that have been hypothesized to produce exospheric refractory gases: impact vaporization, sputtering, and molecular dissociation. However, we later allowed for the possibility of less energetic sources acting upon a limited reservoir of volatile particles because we found that low-altitude data could not be reproduced by high-energy sources. Source processes can be co-added because of the collisionless nature of the exosphere, but they compete for the same surface reservoir. Thermal processes act upon the top monolayer; sputtering affects the top ~10 nm, and impacts tap the top 1 μm or more of the surface.

Sputtering by solar wind ions is a potential source of energetic atoms. Originally introduced to explain the rapid temporal variability and the high-latitude enhancements seen in Mercury's sodium exosphere (e.g., Killen et al., 2001), this source is regulated by the interaction of the solar wind with the magnetosphere formed by Mercury's planetary magnetic field. The fraction of the surface that can be exposed to solar wind ions varies in response mainly to changes in the interplanetary magnetic field (IMF) (e.g., Sarantos et al., 2001; Sarantos et al., 2007). The rate for this source is proportional to three uncertain parameters: the abundance of magnesium in the regolith, the sputtering yield per incident ion, and the influx onto Mercury's surface and composition of the solar wind.

Comment: Menelaos, is this OK?

Impact-driven vaporization caused by micrometeoroids is expected to be a source of exospheric atoms (e.g., Morgan et al. 1988; Cintala 1992; Morgan and Killen, 1997, Killen et al., 2001). The amount of vapor produced in this way is proportional to the influx of micrometeoroids and depends on their velocity distribution. The mean impact velocity may exceed 20 km/s at Mercury's orbit, and is even higher than that for larger meteoroids or during meteoroid streams. Possible temperatures for impact vaporization ejecta of 2500-5000 K, depending on the impact energy and the thermophysical properties of the target material, are obtained in hypervelocity impact experiments (Eichhorn, 1978). Uncertainties in the physical properties of the regolith and the impactors, the assumed micrometeoroid mass flux and velocity, and the method used to calculate the vapor yields each contribute to roughly a factor of five uncertainty in the estimated vapor production rates (e.g., Cintala, 1992; Killen et al., 2005).

Molecules can be produced in the vapor + liquid + solid phase that follows micrometeoroid impact. According to quenching theory, chemical reactions during the collisional phase of the cloud (10^{-7} – 10^{-5} s) lead to the formation of metallic oxides and hydroxides (e.g., MgO, CaO, CaOH) (Berezhnoy and Klumov, 2008; Berezhnoy, 2010). Such molecules may photolyze or dissociate due to their high internal energy and produce high-energy atoms of Mg, Ca, O, as well as other species. We adopt the premise that a dissociating molecule is a major source of energetic atomic Mg (Killen et al., 2010). The same mechanism has been suggested by Killen et al. (2005) to be the main reason why Mercury's neutral Ca tail is extremely hot. Besides the uncertainty in total impact vapor, the unknowns for this source include the abundance ratio of atoms versus molecules of the same species in the vapor cloud, and the molecular dissociation lifetime and temperature.

Although less energetic sources such as photon-stimulated desorption or thermal desorption cannot act on intrinsic magnesium that is bound in silicate phases, such processes could act on recycled, gravitationally returning atoms that were originally vaporized from silicates by impacts and sputtering. The main uncertainty here is whether reabsorbed Mg physisorbs, or weakly adsorbs to the surface following return, so that lower energy processes can re-eject them to the gas phase. The rate for low-energy sources cannot exceed the return rate of atoms delivered by energetic processes, which can be constrained from high-altitude measurements.

4.1.2. Exospheric sinks

Our model explicitly accounts for losses due to ballistic escape and sticking. Each returning atom is assumed to stick with unit efficiency. For those atoms that are generated by a dissociating molecule we also include losses due to the formation of a stable molecule with a finite lifetime (Section 4.4). However, the possible role of the surface as a sink requires some discussion.

Previous investigations have demonstrated that the efficiency of exospheric Na ejection is related to a surface reservoir whose content varies with distance from the Sun. A complex balance between the exospheric and the surface supply arises because (1) the dayside reservoir for the very efficient processes (e.g., thermal vaporization and PSD) can become depleted in local time if the resupply rate is not sufficiently large (Leblanc and Johnson, 2010); (2) the resupply rate is diffusion-limited (Killen et al., 2004; Burger et al., 2010); and (3) solar wind precipitation may enrich the surface by enhancing diffusion through creation of vacancies (Mura et al., 2009; Burger et al., 2010). In sodium simulations by Leblanc and Johnson (2010) and Mura et al. (2009), each test particle is tracked even when trapped at the surface.

Unlike Na, which is a trace species of the regolith, observations of Mg by MESSENGER allow us to infer that the regolith turnover rate ("gardening rate") can most likely provide sufficient fresh targets to populate the exosphere with this species. We demonstrate that only if the impact vapor consists mainly of molecules with half-lives in excess of ~2 min do the required source rates approach the gardening rate (Section 4.4). Otherwise, our results suggest that, to first order, the Mg surface supply for hot processes can be treated as infinite. However, what is limited is a possible reservoir of volatiles which may be needed to explain the measurements at low altitudes (Sections 3 and 5.2). Therefore, we assume in our simulations two populations of Mg at the surface: one that is strongly bound in silicate phases and can be released only by impacts and sputtering, and one that originates from atoms and molecules that have returned to the surface following emission from the silicate population. The latter component should physisorb with lower binding energy than Mg in silicates so that it can be vaporized by lower-energy processes.

Sean Solomon 3/4/11 9:10 AM
Comment: Menelaos, I can't understand this sentence. What is a "thermal particle"? What is your "evidence"?

menelaos sarantos 3/4/11 9:16 AM
Comment: Sean, "volatiles" has substituted "thermal particles". Elsewhere, "thermal processes" are now referred to "low-energy" or "less energetic" processes. I've added the Section numbers where this "evidence" is presented.

4.2. Ion sputtering

Simulations of sputtered magnesium are initialized with the flux of precipitating solar wind ions predicted by a magnetohydrodynamic (MHD) model of Mercury's magnetosphere (Benna et al., 2010). The model predictions under the southward IMF **B** field that prevailed during the second MESSENGER flyby are shown in Fig. 4a. The assumed solar-wind conditions were: $n_{sw} = 20$ cm^{-3}, $V_{sw} = 400$ km/s, and $[B_x, B_y, B_z] = [-$

8, 4, -10] nT, where n_{sw} and V_{sw} are the solar wind density and velocity, respectively, and the IMF is given in Mercury solar orbital coordinates, where x is directed from the center of the planet toward the Sun, z is normal to Mercury's orbital plane and toward the north celestial pole, and y is in the direction opposite to orbital motion.

The production rate due to ion sputtering is obtained by assuming a sputtering yield, Y, weighted by protons and alpha particles, of 0.1 per ion impact (Wurz et al., 2007), an upper limit for the magnesium abundance in the regolith of $c = 0.17$ by number (Wurz et al., 2010), and a precipitating flux of $F_{SW} = 2 \times 10^8$ solar wind ions cm^{-2} s^{-1} poleward of ±50° dayside latitude. These parameters yield a sputtered flux, $F_{SPUTT} = cYF_{SW}$, of 3.6×10^6 Mg atoms cm^{-2} s^{-1} and a modeled near-surface density, n_0, of ~6 atoms cm^{-3} at polar cusp latitudes. The mean ejection energy for this process is approximately half the binding energy, which is assumed to be 3.6 eV in this simulation, and the energy, E, and directionality of the ejecta are described by the Sigmund-Thompson function (e.g., Wurz et al., 2007):

$$f(E,\delta) = \frac{6E_b}{3 - 8\sqrt{E_b / E_{Max}}} \frac{E}{(E + E_b)^3} \{1 - \sqrt{(E + E_b)/E_{Max}}\} \cos\delta \qquad (3)$$

where $E_b = 3.6$ eV the magnesium binding energy to the regolith grains, $E_{Max} = 450$ eV the maximum energy that can be imparted to the ejected magnesium atoms by 3 keV protons, and δ the angle from local vertical. Due to the effects of soil porosity, the atoms are sputtered primarily perpendicular to the surface, with the yield assumed to lessen as cos δ.

Subject to these assumptions, our simulations demonstrate that the contribution by sputtering to the fantail measurements varies from about 10% for observations near the equator to about 50% for those over the northern pole (Fig. 4b). On average, about 20%

of the column abundance observed during these measurements can be attributed to sputtering.

[Insert Fig. 4]

These predictions are uncertain for two reasons. First, the predicted location and flux of the plasma reaching the surface are not only model-dependent but are also sensitive to the assumed solar wind conditions. These conditions can be inferred only indirectly because MESSENGER observes neither the solar wind nor the IMF while inside the magnetosphere. More importantly, the magnetosphere during M2 was extremely dynamic (Slavin et al., 2009), yet the exospheric consequences of short-term (~1 min) magnetospheric variability due to magnetic reconnection have not been evaluated by any model to date. Bearing these uncertainties in mind, we conclude that, although sizeable, the contributions by sputtering alone cannot provide the entire energetic component and so the MESSENGER measurements indicate that some other energetic source process is at play.

4.3. Impact vaporization

To first order the influx of micrometeoroids to Mercury's surface is assumed to be isotropic. We model the production of atomic magnesium during impacts as following a Maxwellian distribution at temperatures 3,000–5,000 K. Under the assumption that meteoroid impacts produce both atoms and molecules, we include in our simulations the dissociation products of $MgO \rightarrow Mg + O$. Three unknowns are the dissociation cross sections, the resulting velocity distribution of the dissociated ejecta, and the molecule lifetime.

Lacking experimental results, we assume that the molecules dissociate due to their high internal energy (they are hot, hence unstable, if they are produced during impacts). In this case, a wide spectrum of ejecta energies can be expected, so our assumed energetic Mg distributions from dissociation are Maxwellian at equivalent temperatures of at least 5,000 K (> 0.5 eV). The dissociation lifetime τ of MgO may be very short, 4 s according to scalings from other diatomic molecules (Berezhnoy, 2010). However, metallic oxides in Earth's atmosphere are fairly stable, with a known lifetime for NaO of 42 s (Self and Plane, 2002). In this Section we present models in which the molecule is assumed to break up immediately upon production ($\tau = 0$) and the exobase is Mercury's surface; in the following section we present models with finite τ, where the exobase is extended.

Sean Solomon 3/4/11 9:16 AM
Comment: Menelaos, you did not include this reference in the References. I have guessed the paper you intended.

menelaos sarantos 3/4/11 9:18 AM
Comment: Sean, you guessed right—thank you.

If $\tau = 0$ and sputtering contributions are small, then we effectively recover the two-component Chamberlain fits (see Table 1) for the partitioning of atoms and molecules in the vapor. A match between the model results and the magnesium measurements in the fantail and near-terminator regions, fit together to describe the global distribution of magnesium self-consistently, is shown in Fig. 5, where "Model Sum" refers to the total contribution by sputtered magnesium, impact-driven atomic magnesium, and magnesium from dissociation. We also ran models where the molecules were allowed to dissociate only on the dayside and beyond the shadow (photolytic scenario), and found, in that case, that the molecule production rates must be about a factor of three higher than the rates quoted in Table 1 to put the same number of atoms in the tail. As in Section 3, the wide range of possible values for these sources can be traced to measurement uncertainties because pairwise combinations of all models differ by statistically insignificant amounts. In summary, we conclude that the high-altitude measurements can be explained by the processes studied here if approximately one-third to one-half of the total amount of exospheric magnesium due to impacts comes directly in atomic form, and the rest results from the dissociation of a molecule, with the total rate summing to (2– 4) × 10^6 Mg atoms cm^{-2} s^{-1} if the molecule photolyzes, or to about (1– 2) × 10^6 Mg atoms cm^{-2} s^{-1} if the molecule vibrationally dissociates.

[Insert Fig. 5]

Can impact vaporization rates produce the observed tail abundances? The total vapor rate produced by micrometeoroid impacts at 0.342 AU was estimated by Killen et al. (2010) to be M_{vap} = 2.7 × 10^7 atoms cm^{-2} s^{-1} for all species. The model is based on the assumption that the delivery of meteoroid material at Earth's vicinity is at a rate of 3 × 10^{-16} g cm^{-3} for particles smaller than 1 cm (Love and Brownlee, 1993); this rate can be scaled to Mercury's distance from the Sun, 0.342 astronomical units (AU) at the time of the second MESSENGER flyby, following Cintala (1992); and the thermodynamic parameters of aluminum onto enstatite and a regolith porosity of 0.5 (Morgan and Killen, 1997; Killen et al., 2005) may be adopted. On assuming a magnesium abundance in the regolith between the lunar values and those recently estimated for Mercury's regolith by Wurz et al. (2010), c = 0.05 – 0.17 by number, we estimate the magnesium production rate due to a uniform micrometeoroid influx to be (1.3–4.7) × 10^6 Mg atoms cm^{-2} s^{-1}. This vaporization rate, which includes the products of MgO if formed in the cloud expansion, is consistent with the rate inferred from the tail measurements, ≤ (2–4) × 10^6 Mg atoms cm^{-2} s^{-1}, if the molecule lifetime is very short. A point that will be studied next, and which was not addressed by Killen et al. (2010), regards the effect of a finite molecule lifetime on impact-driven arguments.

Sean Solomon 3/4/11 9:16 AM
Comment: Menelaos, is "rate" the correct word here, given that you are citing a flux. (See my question at this point in the previous draft.)

4.4. Extended exosphere models

If the molecule has a finite lifetime, the required rates will exceed those quoted above because a fraction of the molecule population returns to the surface before it is dissociated. We tested a source of Mg by dissociation of MgO at different altitudes from the surface. We computed the loss flux to dissociation of MgO molecules as a function of altitude, r, having corrected the distribution function $f(r)$ for the survival probability, $e^{-t(r,v)/\tau}$, where $t(r,v)$ is the time elapsed since ejection from an altitude r_0 and τ the molecule lifetime (e.g., Cui et al., 2008). This loss flux, which is the production rate of new atoms, was used to initialize the atom redistribution model of Eq. 2 where the limits of integration now relate to jumps both from higher and from lower altitudes. The molecule lifetime was treated as a free parameter with an assumed range between 1-1000 s.

Comment: Menelaos, it is not a good idea to have boldface **r** denote radius and italicized *r* denote altitude. I suggest that the pick a different symbol for altitude, say, *z* or *h*.

In the right panel of Fig. 6 we present profiles of the dissociating flux from an MgO molecule produced from the surface at a rate of 10^6 molecules cm^{-2} s^{-1}. On the left the resulting profiles for energetic Mg atoms are shown, along with the $\tau = 0$ profile at the same rate and dissociation temperature. It can be seen that: (1) the profiles from an extended exosphere are less steep, meaning that particles can escape easier from a given altitude at the same assumed dissociation temperature; (2) at $\tau = 1$ s the model approaches the idealized $\tau = 0$ model of the previous section, and (3) if the molecules are stable, higher ejection rates are necessary to populate the tail with the same number of atoms. With the exception of the production rate, the profiles are so similar that we cannot separate the effects of a different temperature of the original molecule (T = 3000 – 5000 K), the different dissociation temperatures (5000 – 20000 K tested), and the different lifetime τ.

menelaos sarantos 3/4/11 9:18 AM
Comment: Sean, is this a clear answer to your question?

Two questions that we can now answer are: can the surface limit the delivery rate of magnesium to the exosphere? And what is the possible lifetime of the putative Mg-bearing molecule? A limit to the rate that the surface can provide is the gardening rate. For a turnover rate at Mercury that is ten times that of the Moon, the top μm is turned over once every 125 years; this rate brings $\sim 6\times10^7$ new Mg atoms cm^{-2} s^{-1} over such a time to the upper μm, which is the depth from which impact vaporization draws its supply. This rate exceeds the exospheric rates by more than an order of magnitude if the molecule has an infinitesimal lifetime (see previous Section). If τ is longer, our simulations indicate that:

- For $\tau = 1000$ s the required source rates to populate the tail exceed the gardening rate.
- For $\tau = 100$ s the data necessitate a rate of (2–5) $\times10^7$ mol cm^{-2} s^{-1}, i.e., less than the gardening rate but up to 10 times the impact vaporization rate given by Cintala (1992).
- For $\tau = 10$ s a best fit requires (3–7) $\times10^6$ mol cm^{-2} s^{-1}, no more than three times the rate quoted in the previous Section.

Our prediction of short dissociation lifetimes for MgO can be tested with laboratory experiments.

5. Magnesium near the surface

We can approximately reproduce the magnesium tail under the assumption that the source processes are sputtering and uniform impact-driven release, but we cannot reproduce the distribution near the terminator where half the exospheric content is not predicted by these processes (compare Fig. 5b to Fig. 3). Because of observational constraints, we cannot ascertain what causes the enhancements observed in this region. We suggest two possibilities that may explain the magnesium distribution near the planetary surface: one relating to a local source of impacts (Section 5.1), and one relating to a reservoir of adsorbed particles (Section 5.2).

5.1. A single ~0.5 m impactor at equatorial dawn?

We can visualize what is inherently different about the measurements obtained near the dawn terminator by mapping with our particle transport model the "footprint" of atoms that scatter light into the instrument for different boresights and tangent heights. Some examples are shown in Fig. 7 for a uniform source having temperature T = 5,000 K.

[Insert Fig. 7]

For lines of sight pointing far from the surface (in the tail and fantail observations), MESSENGER UVVS observed primarily the escaping component; hence the instrument's effective field of view is large. Fig. 7a shows a typical measurement obtained in the tail prior to the spacecraft entering the shadow, and Figs. 7b to 7d show the beginning, middle, and end of the fantail sequence. As expected, the main contributions to the observed column abundance drift from being approximately equally weighted between dawn and dusk in the tail to being primarily dawn, then north, then dusk during the fantail sequence. Particles mapping outside the shadow originate mainly from the nightside surface and contribute approximately two-thirds of the Chamberlain column abundance; ~one-third of the total column abundance is contributed by particles originating on the dayside. (This result implies that the molecule production rates quoted in the paper should be increased by a factor of three if the molecule is destroyed by photons rather than being vibrationally dissociated.). As a wide area of the surface contributes to the tail and fantail measurements, localized "disturbances" such as a surface density enhancement or a meteoroid impinging on Mercury's near-equatorial, morning sector would go undetected until the spacecraft pointed near the surface.

In contrast, for lines of sight nearly intercepting the dawn terminator surface, the ejecta mapping into the instrument's field of view are very localized. As the spacecraft comes out of the shadow, the population sampled is slowly drifting towards the equatorial dawn and morning sectors in successive lines of sight (Fig. 7e – f). We conclude that the measurements near the terminator are sensitive to localized sources. This point is further studied in Fig. 8.

Having evaluated the impact-driven column abundances element by element as in Fig. 7, we then combine them by different amounts to investigate possible asymmetries in a least-squares manner. First, we determine the location of the possible meteoroid impact by iteratively enhancing the weight of "pixels" starting at equatorial dawn, then progressively expanding the "size" of the assumed impact area. The shape of the near-terminator curve is fit best if we enhance only one pixel, that sitting at the dawn terminator with an extent of $\pm$ 10° in longitude and latitude. Then, the production rate and its partitioning into the two impact-driven populations is determined by least-squares regression. This outcome is shown in Fig. 8 for assumed local enhancements of vapor rates over the uniform model by factors of four and eight. As seen in the left column, these models are indistinguishable from fantail measurements, but the models having enhancement factors of 4–8 represent the near-terminator observations increasingly well.

[Insert Fig. 8]

A meteoroid stream is not a suitable explanation because streams would be expected to have a hemispherical dependence and not be so localized (J. Vaubaillon, personal communication, 2010). A single impactor in a small region around dawn is possible. According to our estimates, enhancements of the local impact-driven release rate by factors of 4–8 would require the meteoroid to have a diameter of ~0.3 m; impacts of objects of such a size occur once every 3-4 days at Mercury. The likelihood that this impact happened around dawn within ~1000 s prior to this observation so that the cloud remained localized is low.

5.2. A source of volatile Mg?

An alternative, more likely way to interpret the near-terminator measurements is to assume that returning Mg atoms from an energetic process do not strongly bind with the surface and can be re-emitted to the gas phase when exposed to UV photons or to the high temperatures of the dayside surface. Such a hypothesis is suggested by the two-component Chamberlain fits (Section 3). As illustrated by Fig. 3, a low-energy source produces a sharp increase in column abundance as the spacecraft probes areas near the planet, i.e., within 100 km of the surface. Note, however, that the population consistent with a T = 400 K Chamberlain model would be effectively concentrated on the nightside during this sequence (e.g., see Fig. 7).

A source concentrated on the dayside would produce the same sharp exospheric profile over the terminator but would require much higher source rates than those of a uniform model (Table 1). To investigate the possibility that the terminator measurements for Mg might be consistent with photon-stimulated desorption (PSD) or thermal desorption of adsorbed ejecta, we ran models under the premise that, in addition to uniform impact vaporization of atoms and molecules, sources included a dayside source having a cos (χ) or $\cos^{1/4}$ (χ) dependence on the solar zenith angle, χ, a varying temperature of 100-1500 K, and no emission from the nightside. We found excellent fits to the observed profile for assumed source temperatures of ~700-1200 K. However, the required rates to match the measurements with these dayside source models were too high, 5×10^8 Mg atoms cm^{-2} s^{-1}, to be provided either by the return rate or by the gardening rate; such rates can be justified only if returning particles do not stick and rebound multiple times, which is probably a poor assumption for refractory elements such as Mg.

In conclusion, the illuminated limb-scan profiles can be matched at acceptable source rates only if the putative cold source extends to the nightside. That is, some process other than PSD and thermal desorption would be required to eject low-energy Mg neutrals. Perhaps electron-stimulated desorption (ESD) is responsible for T = 400 K neutrals since magnetospheric electrons have access to the nightside; no ESD measurements are available for this species, however. Note that the inferred rate from a T = 400 K source corresponds to a few times 10^6 atoms cm^{-2} s^{-1} (Table 1). Although our simulations have not carefully treated the reservoir in the top monolayer of the surface, flux of this magnitude could approximately be provided by the return rate of impact-driven atomic Mg and by surface-directed Mg from dissociation of a molecule with a finite lifetime. All but 1–2 % of magnesium atoms from a 3000–5000 K source are gravitationally bound, and approximately half the dissociating flux from a molecule will be directed towards the surface.

6. Conclusions

Comparison of the measurements of Mg in Mercury's exosphere with a large number of simulations have suggested the following possibilities: (1) scale-height arguments imply the presence of at least two distinct temperatures; (2) energetic processes, such as micrometeoroid impact vaporization, ion sputtering, and dissociation of a Mg-bearing oxide, can supply the exospheric population at high altitudes, but no single process dominates; (3) the lifetime of the putative molecule may not exceed ~100 s in order to supply the needed rates given the replenishment rates of the surface by gardening; and (4) at low altitudes, low-energy processes appear to act on a limited reservoir of volatiles that may be provided by recycled atoms from hot processes. A visual summary of the paper's results appears in Fig. 9.

Preliminary analysis of third flyby data (not discussed at length in this paper) indicates similar temperatures and source rates in the tail and polar regions to those presented here. We cannot confirm the volatile source because observations of magnesium on the equatorial dawn region were not conducted by MESSENGER during its third flyby as a result of a spacecraft safe-hold event (Vervack et al., 2010). Improvements to the model will require laboratory measurements of appropriate physical constants (e.g., molecule lifetime and dissociation cross-sections, and temperature-programmed desorption yields for adsorbed Mg). The measurements expected during the orbital phase of the MESSENGER mission promise to further constrain these results. For instance, if impacts populate the high-altitude Mg exosphere as inferred here, there should be a correlation of exospheric content with spacecraft passages through the interplanetary dust plane (Kameda et al., 2009). A source of volatiles can be verified or refuted during repeated illuminated limb-scanning opportunities.

Acknowledgments. The MESSENGER project is supported by the NASA Discovery Program under contracts NAS5-97271 to the Johns Hopkins University Applied Physics Laboratory and NASW-00002 to the Carnegie Institution of Washington. RMK, RJV, and MB are supported by the MESSENGER Participating Scientist Program. MS thanks Apostolos Christou and Jeremie Vaubaillon for their remarks on the possibility that a meteoroid stream affected Mercury during the flyby observations, and Richard Hartle for his suggestions on modeling exospheric dissociating ejecta.

References

Sean Solomon 2/4/11 9:16 AM
Comment: Menelaos, in PSS journal names are not set in italics; no comma precedes the volume number, and volumes numbers are neither in italics or boldface.

Benna, M., Anderson, B.J., Baker, D.N., Boardsen, S.A., Gloeckler, G., Gold, R.E., Ho, G.C., Killen, R.M., Korth, H., Krimigis, S.M., Purucker, M.E., McNutt, R.L., Jr., Raines, J.M., McClintock, W.E., Sarantos, M., Slavin, J.A., Solomon, S.C., Zurbuchen, T.H., 2010. Modeling of the magnetosphere of Mercury at the time of the first MESSENGER flyby. Icarus 209, 3–10.

Berezhnoy, A.A., 2010. Meteoroid bombardment as a source of the lunar exosphere. Adv. Space Res. 45, 70–76.

Berezhnoy, A.A., Klumov, B.A., 2008. Impacts as sources of the exosphere on Mercury. Icarus 195, 511–522.

Burger, M.H., Killen, R.M., Vervack, R.J., Jr., Bradley, T.E., McClintock, W.E., Sarantos, M., Benna, M., Mouawad, N., 2010. Monte Carlo modeling of sodium in Mercury's exosphere during the first two MESSENGER flybys. Icarus 209, 63–74.

Chamberlain, J.W., 1963. Planetary coronae and atmospheric evaporation. Planet. Space Sci. 11, 901–960.

Cintala, M.E., 1992. Impact-induced thermal effects in the lunar and Mercurian regoliths. J. Geophys. Res. 97, 947–973.

Cui, J., Yelle, R.V., Volk, K., 2008. Distribution and escape of molecular hydrogen in Titan's thermosphere and exosphere. J. Geophys. Res. 113, E10004, doi:10.1029/2007JE003032.

Eichorn, G., 1978. Heating and vaporization during hypervelocity particle impact. Planet. Space Sci. 26, 463–467.

Hartle, R.E., 1971. Model for rotating and nonuniform planetary exospheres. Phys. Fluids 14, 2592–2598.

Kameda, S., Yoshikawa, I., Kagitani, M., Okano, S., 2009. Interplanetary dust distribution and temporal variability of Mercury's atmospheric Na. Geophys. Res. Lett. 36, L15201, doi:10.1029/2009GL039036.

Killen, R.M., Potter, A.E., Reiff, P., Sarantos, M., Jackson, B.V., Hick, P., Giles, B., 2001. Evidence for space weather at Mercury. J. Geophys. Res. 106, 20509–20526.

Killen, R.M., Sarantos, M., Potter, A.E., Reiff, P.H., 2004. Source rates and ion recycling rates for Na and K in Mercury's atmosphere. Icarus 171, 1–19.

Killen, R.M., Bida, T.A., Morgan, T.H., 2005. The calcium exosphere of Mercury. Icarus 173, 300–311.

Killen, R.M., Cremonese, G., Lammer, H., Orsini, S., Potter, A.E., Sprague, A.L., Wurz, P., Khodachenko, M.L., Lichtenegger, H.I.M, Milillo, A., Mura, A., 2007. Processes that promote and deplete the atmosphere of Mercury. Space Sci. Rev. 132, 433–509.

Killen, R.M., Shemansky, D., Mouawad, N., 2009. Expected emission from Mercury's exospheric species, and their ultraviolet-visible signatures. Astrophys. J. Suppl. Ser. 181, 351–359.

Killen, R.M., Potter, A.E., Vervack, R.J., Jr., Bradley, E.T., McClintock, W.E., Anderson, C.M., 2010. Observations of metallic species in Mercury's exosphere. Icarus 209, 75–87.

Leblanc, F., Johnson, R.E., 2010. Mercury exosphere I. Global circulation model of its sodium component. Icarus 209, 280–300.

Love, S.G., Brownlee, D.E., 1993. A direct measurement of the terrestrial mass accretion rate of cosmic dust. Science 262, 550–553.

McClintock, W.E., Bradley, E.T., Vervack, R.J., Jr., Killen, R.M., Sprague, A.L., Izenberg, N.R., Solomon, S.C., 2008. Mercury's exosphere: observations during MESSENGER's first Mercury flyby. Science 321, 92–94.

McClintock, W.E., Vervack, R.J. Jr., Bradley, E.T., Killen, R.M., Mouawad, N., Sprague, A.L., Burger, M.H., Solomon, S.C., Izenberg, N.R., 2009. MESSENGER observations of Mercury's exosphere: detection of magnesium and distribution of constituents. Science 324, 610–613.

Milillo, A., Fujimoto, M., Kallio, E., Kameda, S., Leblanc, F., Narita, Y., Cremonese, G., Laakso, H., Laurenza, M., Massetti, S., McKenna-Lawlor, S., Mura, A., Nakamura, R., Omura, Y., Rothery, D.A., Seki, K., Storini, M., Wurz, P., Baumjohann, W., Bunce, E.J., Kasaba, Y., Helbert, J., Sprague, A.L., 2010. The BepiColombo mission: an outstanding tool for investigating the Hermean environment. Planet. Space Sci. 58, 40–60.

Morgan, T.H., Killen, R.M., 1997. A non-stoichiometric model of the composition of the atmospheres of Mercury and the Moon. Planet. Space Sci, 45, 81–94.

Morgan, T.H., Zook, H.A., Potter, A.E., 1988. Impact-driven supply of sodium and potassium to the atmosphere of Mercury. Icarus 75, 156–170.

Mouawad, N., Burger, M.H., Killen, R.M., Potter, A.E., Naidu, S., McClintock, W.E., Vervack, R.J. Jr., Bradley, E.T., 2011. Constraints on Mercury's sodium exosphere: Combined MESSENGER and ground – based data. Icarus 211, 21–36.

Mura, A., Wurz, P., Lichtenegger, H.I.M., Schleicher, H., Lammer, H., Delcourt, D., Milillo, A., Orsini, S., Massetti, S., Khodachenko, M.L., 2009. The sodium exosphere of Mercury: comparison between observations during Mercury's transit and model results. Icarus 200, 1–11.

Sarantos, M., Reiff, P.H., Hill, T.W., Killen, R.M., Urquhart, A.L., 2001. A B_x-interconnected magnetosphere model for Mercury. Planet. Space Sci. 49, 1629–1635.

Sarantos, M., Killen, R.M., Kim, D., 2007. Predicting the long-term solar wind ion-sputtering source at Mercury. Planet. Space Sci. 55, 1584–1595.

Sarantos, M., Killen, R.M., Sharma, A.S., Slavin, J.A., 2010. Sources of sodium in the lunar exosphere: modeling using ground-based observations and spacecraft data of the plasma. Icarus 205, 364–374.

Self, D.E., Plane, J.M.C., 2002. Absolute photolysis cross-sections for $NaHCO_3$, NaOH, NaO, NaO_2 and NaO_3: implication for sodium chemistry in the upper mesosphere. Phys. Chem. Chem. Phys. 4, 16–23.

Slavin, J.A., Acuña, M.H., Anderson, B.J., Baker, D.N., Benna, M., Boardsen, S.A., Gloeckler, G., Gold, R.E., Ho, G.C., Korth, H., Krimigis, S.M., McNutt, R.L., Jr., Raines, J.M., Sarantos, M., Schriver, D., Solomon, S.C., Trávníček, P., Zurbuchen, T.H., 2009. MESSENGER observations of magnetic reconnection in Mercury's magnetosphere. Science 324, 606–610.

Solomon, S.C., McNutt, R.L., Jr., Gold, R.E., Acuña, M.H., Baker, D.N., Boynton, W.V., Chapman, C.R., Cheng, A.F., Gloeckler, G., Head, J.W., III, Krimigis, S.M., McClintock, W.E., Murchie, S.L., Peale, S.J., Phillips, R.J., Robinson, M.S., Slavin, J.A., Smith, D.E., Strom, R.G., Trombka, J.I., Zuber, M.T., 2001. MESSENGER mission to Mercury: scientific objectives and implementation. Planet. Space Sci. 49, 1445–1460.

Vervack, R.J., Jr., McClintock, W.E., Killen, R.M., Sprague, A.L., Anderson, B.J., Burger, M.H., Bradley, E.T., Mouawad, N., Solomon, S.C., Izenberg, N.R., 2010. Mercury's complex exosphere: results from MESSENGER's third flyby. Science 329, 672–675.

Wurz, P., Rohner, U., Whitby, J.A., Kolb, C., Lammer, H., Dobnikar, P., Martín-Fernández, J.A., 2007. The lunar exosphere: the sputtering contribution. Icarus 191, 486–496.

Wurz, P., Whitby, J.A., Rohner, U., Martín-Fernández, J.A., Lammer, H., Kolb, C., 2010. Self-consistent modelling of Mercury's exosphere by sputtering, micro-meteorite impact and photon-stimulated desorption. Planet. Space Sci. 58, 1599–1616.

Table 1. Two-component Chamberlain models obtained by superposing a cool source, 100-5000 K, and a hot source, $T \geq 10000$ K.

Model: $n_{0,\mathrm{LT}}\ I(T=3000\ \mathrm{K}) + n_{0,\mathrm{HT}}\ I(T)$					
$n_{0,\mathrm{LT}}$ (atoms cm^{-3})	T ($\times10^3$ K)	$n_{0,\mathrm{HT}}$ (atoms cm^{-3})	S_{LT} ($\times10^5$ cm^{-2} s^{-1})	S_{HT} ($\times10^6$ cm^{-2} s^{-1})	χ^2/ν
6.1	10	12.7	2.4	0.9	6.23
14.8	20	8.7	6.0	1.0	5.48
16.8	30	8.5	6.8	1.1	5.29
17.7	40	8.7	7.2	1.3	5.20
18.1	50	9.0	7.4	1.5	5.15
Model: $n_{0,\mathrm{LT}}\ I(T=400\ \mathrm{K}) + n_{0,\mathrm{HT}}\ I(T)$					
$n_{0,\mathrm{LT}}$ (atoms cm^{-3})	T ($\times10^3$ K)	$n_{0,\mathrm{HT}}$ (atoms cm^{-3})	S_{LT} ($\times10^6$ cm^{-2} s^{-1})	S_{HT} ($\times10^6$ cm^{-2} s^{-1})	χ^2/ν
298	10	12.1	4.4	0.9	5.87
397	20	9.0	5.9	0.9	5.03
418	30	8.9	6.2	1.1	4.84
426	40	9.2	6.3	1.4	4.75
430	50	9.5	6.4	1.6	4.71

Notes: Listed are the corresponding surface density, n_0, production rate, S, and reduced chi squared error, χ^2/ν, for different assumed values of the exobase temperature, T. The models are fit to all measurements. (LT=Low Temperature; HT = High Temperature)

Figure Captions .

Fig. 1. All Mg observations obtained during MESSENGER's second flyby were fit to Chamberlain models. Shown here are lines of sight through the tail that intercept the noon-midnight meridian plane (a) 2 to 4 R_M from the equatorial plane; (b) 1 to 2 R_M from the equator; and (c) inside Mercury's shadow. The measurements and their uncertainties are shown in red. Three models shown, which have temperatures of 3,000 (dotted black line), 20,000 (blue line) and 50,000 K (magenta line), indicate that atoms in the tail are very energetic.

Fig. 2. Weighted least-squared fits of (a) the fantail and (b) near-terminator measurements to Chamberlain models subject also to the tail data. Only a poor description of the low-altitude measurements near dawn can be achieved with a single temperature.

Fig. 3. Two-component models are improvements over single-component models at low altitudes, especially if a low-energy source (T = 400 K) is assumed (panels c and d). The fantail observations, where the line of sight drifts to infinity, constrain the energetic process, whereas the source having the smaller temperature dominates the near-terminator measurements, which probe altitudes near the surface.

Fig. 4. (a) The adopted location and flux of protons bombarding the surface of Mercury, obtained from a MHD model of Mercury's magnetosphere (Benna et al., 2010); (b) amount of magnesium that can be attributed to sputtering under these conditions.

Fig. 5. A possible model of Mercury's magnesium exosphere consisting of three assumed source processes: sputtering (in green), impact vaporization of atomic Mg (in black), and dissociation of MgO (in blue). In contrast to the model shown in the next figure, here the molecule is assumed to break up immediately upon production ($\tau = 0$). In this limiting case the inferred rates can be provided by impact vaporization of atoms and molecules for magnesium abundances in the regolith of five percent or higher. The sputtering contribution to the near-terminator measurements is below the scale shown.

Fig. 6. (a) Flux of dissociating MgO as a function of radial distance and an assumed molecule lifetime, τ, as the source rate for an extended exosphere model; (b) profiles of energetic Mg resulting from the dissociation of MgO with arbitrary τ. A production rate of 10^6 molecules cm^{-2} s^{-1} and a dissociation temperature of 20,000 K are assumed; $\tau = 0$ is the profile used in the simplified case of Fig. 5 at the same temperature. Ejection rates of a stable molecule must evidently be higher in order to produce the same column abundance in the tail. Based on a comparison to the gardening rate, the molecule must be short-lived, $\tau \leq 2$ min, to explain the measurements.

Fig. 7. Relative contribution by planetary surface elements to the modeled column abundance for an isotropic impact vaporization source ($T = 5000$ K) and for selected lines

of sight: (a) typical line through the equatorial tail when the spacecraft lies outside the shadow; (b)-(d) the beginning, mid-point, and end of the fantail sequence; (e)-(f) first and last lines of sight for the near-terminator sequence. In these plots, the integrated column abundance from a model of uniform ejection has been divided to extract the originating locations of particles that map outside the planetary shadow (and hence contribute to the measurements). The main point illustrated is that particles that affect the pre-dawn observations originate from a limited region nearby. The subsolar point is indicated by the white dot.

Fig. 8. In addition to the assumption of a low-energy source (Fig. 3), models of the near-terminator measurements markedly improve if a single meteoroid impacted Mercury within $\pm 10°$ of equatorial dawn around the time of these observations: (upper panel) model with no equatorial enhancement at dawn; (middle panel) model with a factor of four, and (lower panel) model with a factor of eight enhancement over the uniform impact vaporization rate. In each case the "background" surface density, n_0, needed to match the data is shown in black ($T = 3000$ K) and blue ($T = 20{,}000$ K). It is surmised that a single meteoroid should have produced the equivalent flux of $\sim(6\text{–}8) \times 10^6$ atoms/molecules cm^{-2} s^{-1} within a brief period prior to the last few measurements for this scenario to work.

Fig. 9. Schematic depiction of potential processes promoting Mg to the exosphere. The gardening rate in the top micron suffices to provide the exospheric rates, shown here for

brief molecule lifetimes. The recycling rate of bound ejecta could replenish an unexpected reservoir of volatiles at rates of ~10^6 atoms cm^{-2} s^{-1}.

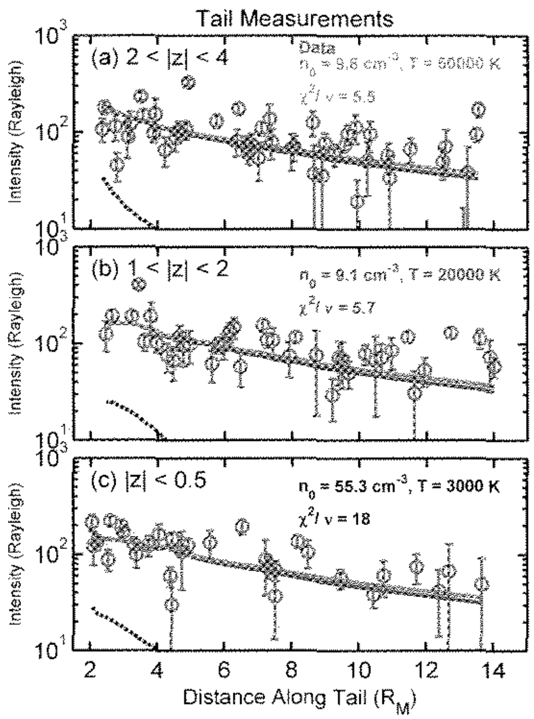

Figure. 1

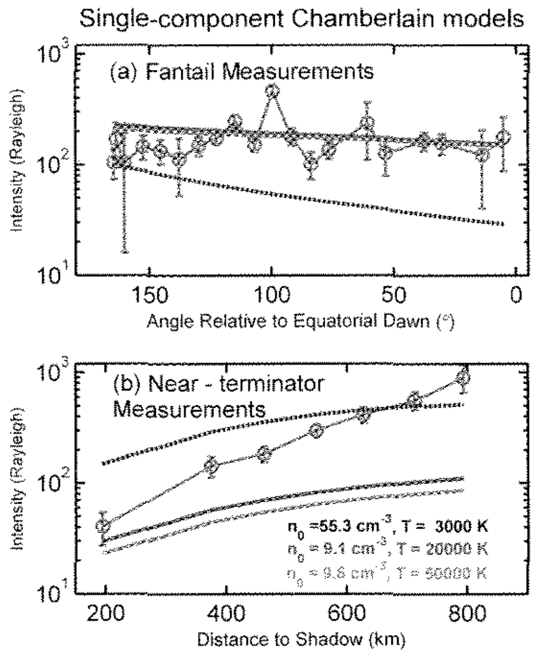
Single-component Chamberlain models
(a) Fantail Measurements
Intensity (Rayleigh)
Angle Relative to Equatorial Dawn (°)
(b) Near - terminator Measurements
Distance to Shadow (km)
n0 =55.3 cm-3, T = 3000 K
n0 = 9.1 cm-3, T = 20000 K
n0 = 9.6 cm-3, T = 50000 K

Figure 2

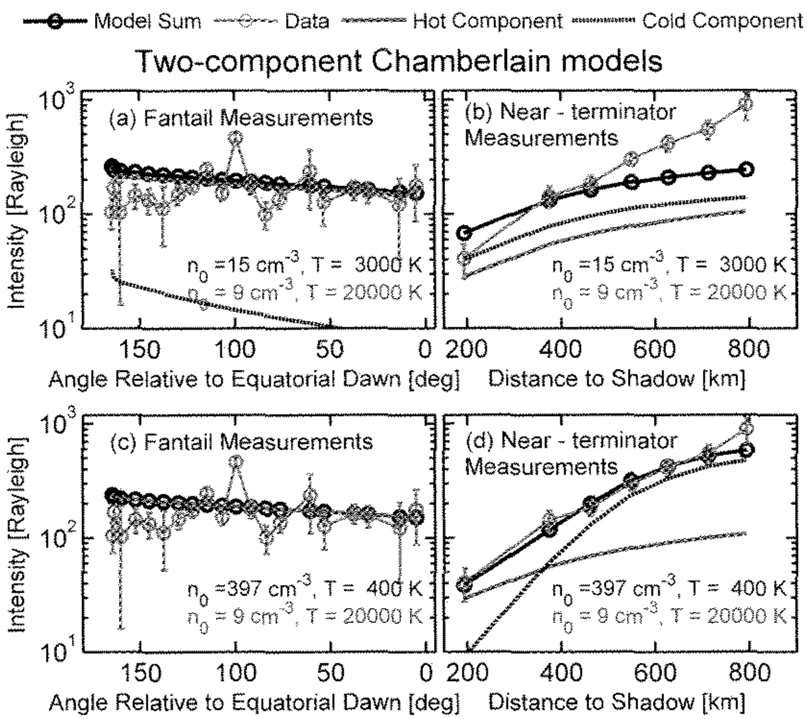
Model Sum
Data
Hot Component
Cold Component
Two-component Chamberlain models
(a) Fantail Measurements
(b) Near - terminator Measurements
(c) Fantail Measurements
(d) Near - terminator Measurements
Intensity [Rayleigh]
n0 =15 cm-3, T = 3000 K
n0 = 9 cm-3, T = 20000 K
n0 =397 cm-3, T = 400 K
Angle Relative to Equatorial Dawn [deg]
Distance to Shadow [km]

Figure 3

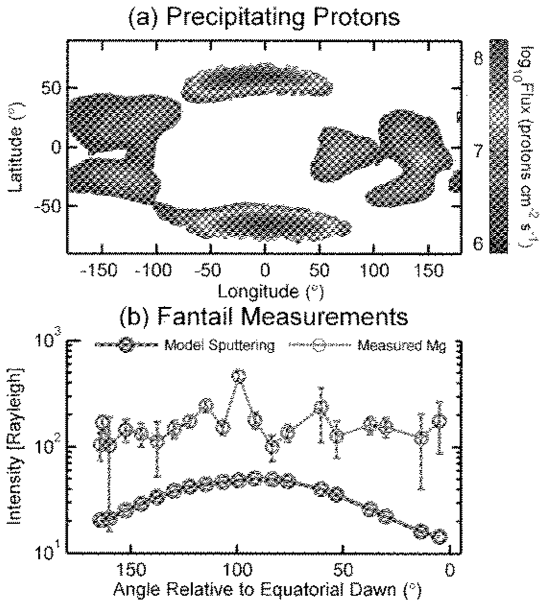
(a) Precipitating Protons
Latitude (°)
Longitude (°)
log10Flux (protons cm-2 s-1)
(b) Fantail Measurements
Model Sputtering
Measured Mg
Intensity [Rayleigh]
Angle Relative to Equatorial Dawn (°)

Figure 4

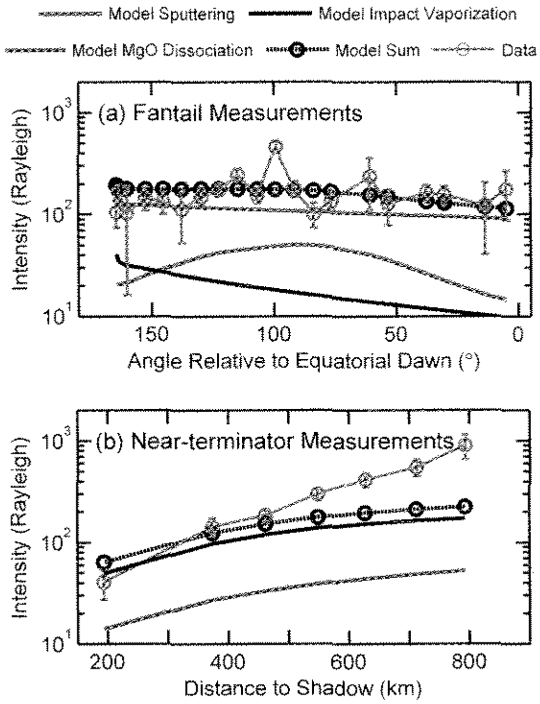

Figure 5

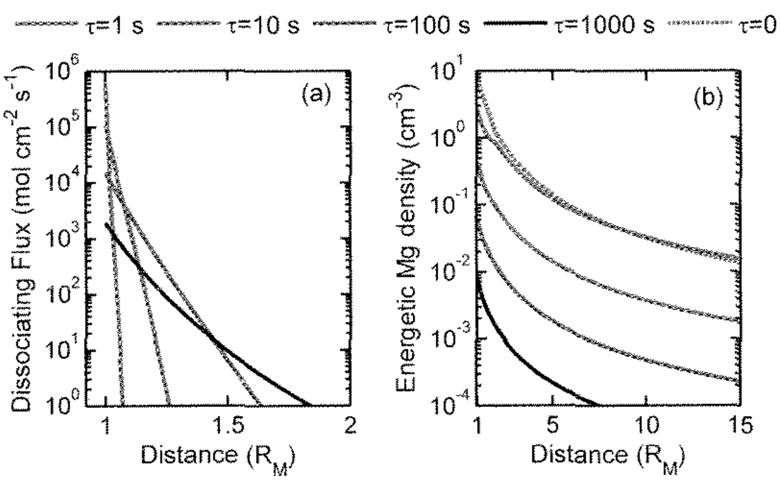

Figure 6

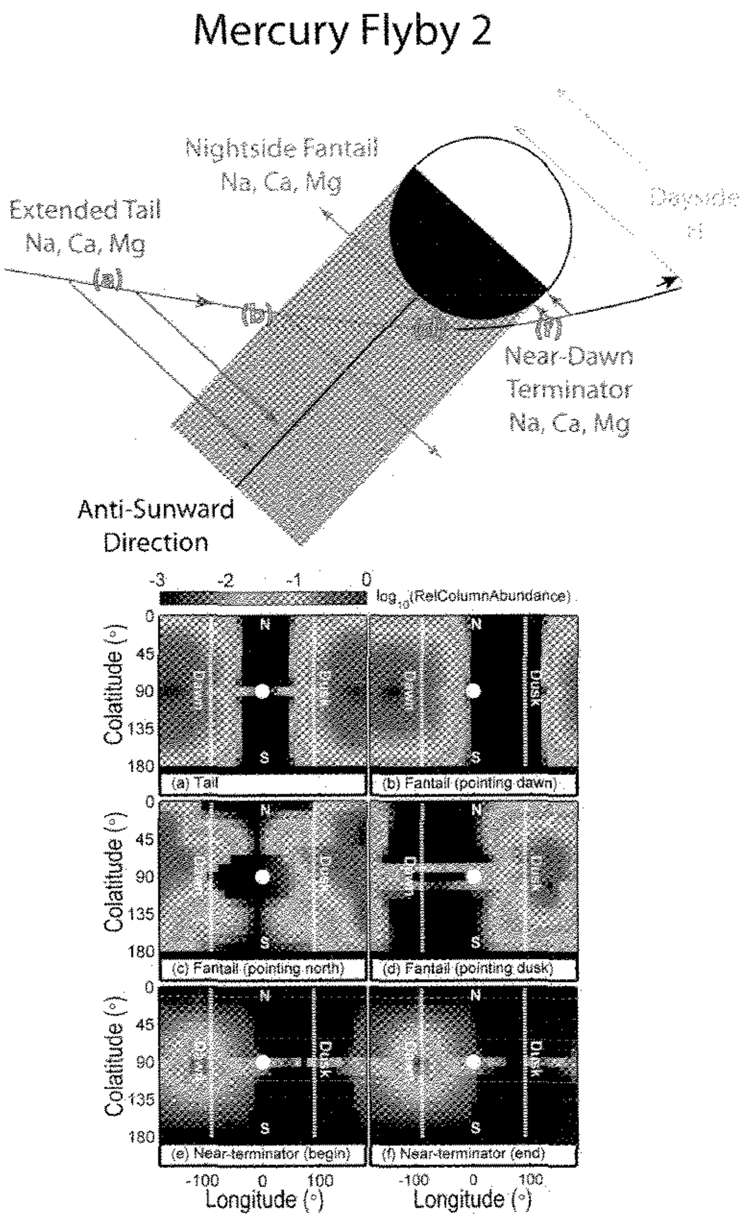
Mercury Flyby 2
Nightside Fantail
Na, Ca, Mg
Extended Tail
Na, Ca, Mg
(a)
(b)
(d)
(f)
Near-Dawn
Terminator
Na, Ca, Mg
Anti-Sunward
Direction
log10(RelColumnAbundance)
Colatitude (°)
Longitude (°)
(a) Tail
(b) Fantail (pointing dawn)
(c) Fantail (pointing north)
(d) Fantail (pointing dusk)
(e) Near-terminator (begin)
(f) Near-terminator (end)

Figure 7

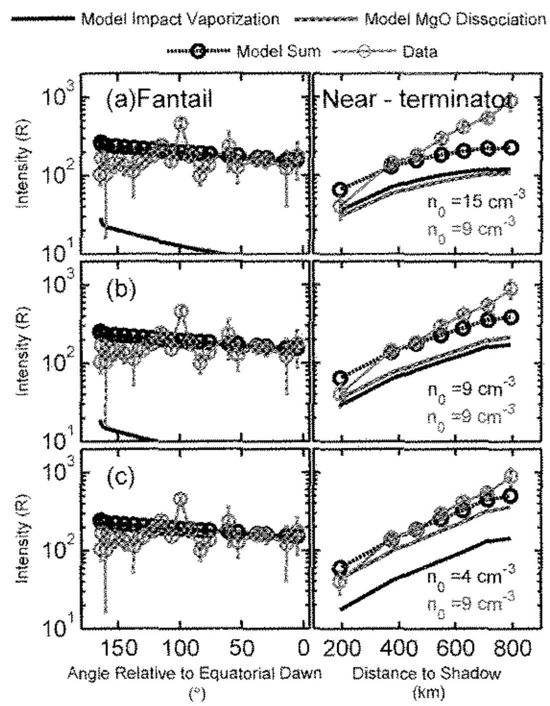

802

803 Figure 8

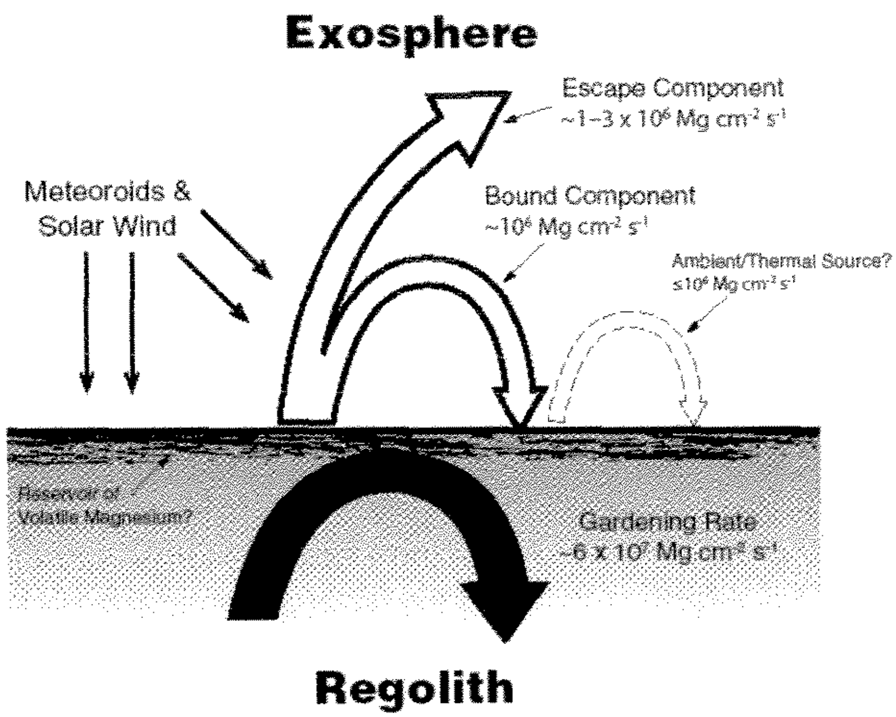
Exosphere
Escape Component
~1–3 x 10^6 Mg cm^{-2} s^{-1}
Meteoroids &
Solar Wind
Bound Component
~10^6 Mg cm^{-2} s^{-1}
Ambient/Thermal Source?
≤10^6 Mg cm^{-2} s^{-1}
Reservoir of
Volatile Magnesium?
Gardening Rate
~6 x 10^7 Mg cm^{-2} s^{-1}
Regolith

Figure 9